Anatomy of charged grain boundaries in polycrystalline solar cells

Benoit Gaury
Center for Nanoscale Science and Technology, National Institute of Standards and Technology, Gaithersburg, MD 20899, USA and Maryland NanoCenter, University of Maryland, College Park, MD 20742, USA

Paul M. Haney
Center for Nanoscale Science and Technology, National Institute of Standards and Technology, Gaithersburg, MD 20899, USA

(Dated: April 17, 2017)

We present analytical relations for the dark recombination current of a pn^+ junction with positively charged columnar grain boundaries in the high defect density regime. We consider two defect state configurations relevant for positively charged grain boundaries: a single donor state and a continuum of both acceptors and donors. Compared to a continuum of acceptor+donor states, or to the previously studied single acceptor+donor state, the grain boundary recombination of a single donor state is suppressed by orders of magnitude. We show numerically that superposition holds near the open-circuit voltage $V_{\rm oc}$, so that our dark $J(V)$ relations determine $V_{\rm oc}$ for a given short circuit current $J_{\rm sc}$. We finally explicitly show how $V_{\rm oc}$ depends on the grain boundary defect state structure.

arXiv:1704.04234v1 [cond-mat.mes-hall] 12 Apr 2017

I. INTRODUCTION

Polycrystalline thin film photovoltaic materials exhibit high power conversion efficiency despite their high defect density[1]. Solar cells based on these materials show high carrier collection but still suffer from recombination losses which limit the open-circuit voltage.[2] Despite the recent progress in exceeding the 20 % efficiency mark[3] (mostly because of improved light management[4]), questions remain on the precise transport mechanisms at play in these systems, and in particular on the role of grain boundaries, which remains unclear. These high efficiencies reveal the need for a fuller understanding of grain boundary properties and their impact on charge transport and recombination.

Even though interpretation of nanoscale measurements is often challenging, a majority of experimental works provide evidence for positively charged grain boundaries in CdTe[5–7]. Previous numerical simulations[8–11] found that charged grain boundaries reduce the open-circuit voltage $V_{\rm oc}$, in agreement with the observation that the $V_{\rm oc}$ of these systems falls significantly short of the theoretical maximum.[12] In order to develop a more quantitative understanding of the relations between microscopic charge transport and macroscopic observables, numerical modeling needs to be complemented by analytical descriptions.

In this work we focus on a pn^+ junction with positively charged, columnar grain boundaries, and provide analytical expressions for the grain boundary dark current. The analysis of Ref. 13 is generalized to two different sources of positive grain boundary charge: a single donor defect state in the gap, and a continuum of both acceptor and donor states. Compared to a continuum of acceptor+donor states, or to the previously studied single acceptor+donor state, the grain boundary recombination of a single donor state is suppressed by orders of magnitude. We further provide physical descriptions of the reduction of $V_{\rm oc}$ by grain boundaries, with a closed form expression for $V_{\rm oc}$. We found that the enhanced recombination for the continuum of gap states results in a reduction of $V_{\rm oc}$ that depends quantitatively on the distribution of donor and acceptor states. The scope of this analysis is limited to grains that are not fully depleted (i.e. independent boundaries), and materials with large hole mobility.

There are many qualitative similarities between the behavior of the single donor+acceptor considered in Ref. 13 and the single donor and continuum cases studied here. In all cases, there are three regimes of qualitatively distinct behavior, which can roughly be classified according to the grain boundary core type: n-type, p-type, or neither (the latter case applies at high applied voltages, where both electron and hole densities vary with voltage). The full explicit form of the grain boundary dark current is shown in Table I for all defect configurations. An important new finding in this work is the reduction of grain boundary recombination by the removal of acceptor states.

This article is structured as follows. We begin with a description of the physical model for the grain boundary, encompassing both the single donor case and the continuum of gap states in Sec. II. We summarize the equilibrium properties of the grain boundary and our assumptions for analyzing the out-of-equilibrium problem in Sec. III. We present the charge transport and associated grain boundary dark current for the single donor state in Sec. IV, and for the continuum of gap states in Sec. V. We end the article with Sec. VI where we discuss the implications of our analysis on the open-circuit voltage of an illuminated pn junction. Finally, we examine the differences between the various configurations of the gap states throughout the paper.

Grain boundary dark current: $J_{\mathrm{GB}}(V) = \lambda \frac{S}{d} N e^{-E_a/k_B T} e^{qV/(nk_B T)}$				
Defect(s)	Param.	n-type	p-type	high-recombination
single D	n	1	1	2
	E_a	E_{GB}	$E_g - E_{\mathrm{GB}}$	$E_g/2$
	N	N_V	N_C	$\sqrt{N_C N_V}$
	S	$(1-f_0)S_p$	S_n	$\sqrt{(1-f_0)S_n S_p}$
	λ	L_{GB}	L_{GB} for $L_n \gg L_{\mathrm{GB}}$ L_n for $L_n \ll L_{\mathrm{GB}}$	L_{GB} for $L'_n \gg L_{\mathrm{GB}}$ L'_n for $L'_n \ll L_{\mathrm{GB}}$
single A+D	n	1	1	2
	E_a	E_{GB}	$E_g - E_{\mathrm{GB}}$	$E_g/2$
	N	N_V	N_C	$\sqrt{N_C N_V}$
	S	$S_p/2$	$S_n/2$	$\sqrt{S_n S_p}/2$
	λ	L_{GB}	L_{GB} for $L_n \gg L_{\mathrm{GB}}$ x_0 for $L_n \ll L_{\mathrm{GB}}$	L_{GB} for $L'_n \gg L_{\mathrm{GB}}$ L'_n for $L'_n \ll L_{\mathrm{GB}}$
Continuum A+D	n	1	1	2
	E_a	E_{GB}	$E_g - E_{\mathrm{GB}}$	$E_g/2$
	N	N_V	N_C	$\sqrt{N_C N_V}$
	S	$\mathcal{S}_p$	$\mathcal{S}_n$	$\mathcal{S}/\sqrt{\gamma}$
	λ	L_{GB}	L_{GB} for $L_n \gg L_{\mathrm{GB}}$ x_0 for $L_n \ll L_{\mathrm{GB}}$	L_{GB} for $L'_n \gg L_{\mathrm{GB}}$ L'_n for $L'_n \ll L_{\mathrm{GB}}$

TABLE I. Summary of analytical results for the grain boundary recombination current for various defect density of states (single donor, single donor and acceptor, continuum of donors and acceptors). The general form of the grain boundary dark current is $J_{\mathrm{GB}}(V) = \lambda S/dN e^{-E_a/k_B T} e^{qV/(nk_B T)}$ where S is a surface recombination velocity, λ is a length characteristic of the recombination region, N is an effective density of states, E_a is an activation energy, n is the ideality factor and V is the applied voltage. Each column corresponds to the regime in which the grain boundary is depending on voltage. L_{GB} is the length of the grain boundary, L_n and L'_n are effective electron diffusion lengths, x_0 is given by Eq. (64). f_0 is the thermal equilibrium occupancy of the single donor state ($f_0 \approx 1$). γ is given by Eq. (48)

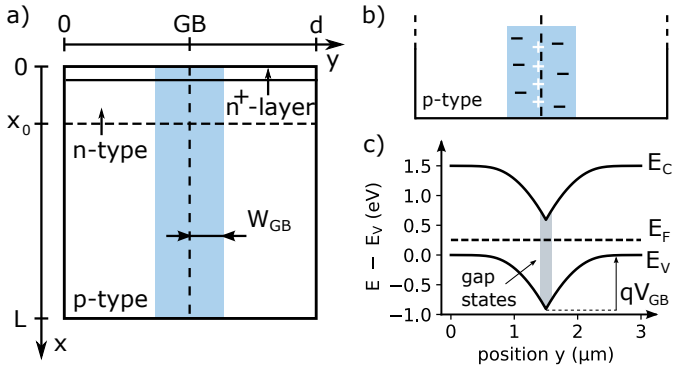

FIG. 1. (a) 2D model system of a pn^+ junction containing a columnar grain boundary. The depletion region of the grain boundary is indicated in blue (width $2W_{\mathrm{GB}}$). x_0 is the point in the grain interior where electron and hole densities are equal. (b) Static charges at and around the grain boundary core (+ and − signs respectively) in the p-type part of the system. (c) Schematic of a band structure corresponding to the situation described in (b).

II. PHYSICAL MODEL OF THE GRAIN BOUNDARY

Our model system is depicted in Fig. 1(a): a pn^+ junction of width d and length L with a grain boundary perpendicular to the junction. We use periodic boundary conditions in the y-direction so that the system describes a closed grain of width d ($d = 3$ μm in our numerical calculations). We assume selective contacts such that the electron (hole) current vanishes at $x = L$ ($x = 0$). We define x_0 as the position where electron and hole concentrations are equal in the grain interior. As stated in introduction we focus on positively charged grain boundaries, which require screening by nearby negative charges (free electrons or ionized acceptor dopants) to conserve the device electroneutrality. The consequences of the screening on the electrostatics surrounding the grain boundary depend on the statistics of the gap levels, the defect density of states, and on the grain interior type (n-type or p-type region). For example, a p-type material will develop an electric field around the grain boundary to repel free holes from the grain boundary core, creating a depleted region around it. Because of the absence of holes, this region has a negative charge compensating the positive charge of the defect, as shown in Fig. 1(b). Electroneutrality determines the extent of this depleted region: the net charge (grain boundary charge plus depleted charge) of the ensemble grain boundary/depletion region is zero.

The consequence of the aforementioned electric field on the local energy landscape can be seen on a band structure plot across the grain boundary, as shown in Fig. 1(c). The electric field leads to the bending of the conduction and valence bands, leading to a built-in potential V_{GB} around the grain boundary. Depending on materials parameters and the extent of band bending, the grain boundary core may undergo type inversion with respect to the grain interior. Each grain boundary type has different carrier transport properties under nonequilibrium conditions. In this work we consider both inverted and non-inverted grain boundaries.

The grain boundary is modeled as a two-dimensional plane with various concentrations of donor and acceptor gap states. The grain boundary charge density reads

$$Q_{\mathrm{GB}} = q \int_0^{E_g} \mathrm{d}E \; \rho_D(E)\,[1 - f_D(E)] - \rho_A(E) f_A(E), \tag{1}$$

where ρ_D (ρ_A) is a two-dimensional density of donor (acceptor) states per energy unit. The occupancies of each donor/acceptor state (indicated by the index $k \in (D, A)$) is[14]

$$f_k(E) = \frac{S_n^k n_{\mathrm{GB}} + S_p^k \bar{p}_{\mathrm{GB}}(E)}{S_n^k (n_{\mathrm{GB}} + \bar{n}_{\mathrm{GB}}(E)) + S_p^k (p_{\mathrm{GB}} + \bar{p}_{\mathrm{GB}}(E))}, \tag{2}$$

where n_{GB} (p_{GB}) is the electron (hole) carrier density at the grain boundary, S_n (S_p) is the electron (hole) surface

recombination velocity, $\bar{n}_{\rm GB}$ and $\bar{p}_{\rm GB}$ are

$$\bar{n}_{\rm GB}(E) = N_C e^{(-E_g+E)/k_BT} \quad (3)$$

$$\bar{p}_{\rm GB}(E) = N_V e^{-E/k_BT} \quad (4)$$

where E is a defect energy level calculated from the valence band edge, N_C (N_V) is the conduction (valence) band effective density of states, E_g is the material bandgap, k_B is the Boltzmann constant and T is the temperature. The parameters $S^k_{n,p}$ and ρ_k are related to the electron and hole capture cross sections $\sigma^k_{n,p}$ by $S^k_{n,p} = \sigma^k_{n,p} v_t \int_0^{E_g} {\rm d}E\ \rho_k(E)$, where v_t is the thermal velocity. In this work we vary $S^k_{n,p}$ with fixed ρ_k; this corresponds to varying $\sigma^k_{n,p}$ accordingly. Note that at thermal equilibrium Eq. (2) reduces to the Fermi-Dirac distribution, and is independent of the recombination velocity parameters. In this case the occupancies of donor and acceptor states at energy E are equal, which we denote by $f_{\rm GB}(E)$ where $f_{\rm GB}(E) = (1+\exp[(E-E_F)/k_BT])^{-1}$.

In this work we restrict the scope of Eq. (1) to two cases of interest for positively charged grain boundaries. First, we focus on a single donor state at $E_{\rm GB}$: $\rho_D(E) = N_{\rm GB}\delta(E-E_{\rm GB})$, where $N_{\rm GB}$ is a two-dimensional defect density (units of m^{-2}). Denoting $f_0 = f_{\rm GB}(E_{\rm GB})$, the grain boundary charge reads

$$Q_{\rm GB} = qN_{\rm GB}(1-f_0). \quad (5)$$

Our second case is a continuum of uniform densities of acceptor and donor states in the gap: $\rho_D(E) = N_{\rm GB}/E_g$, $\rho_A(E) = \alpha N_{\rm GB}/E_g$. α is the ratio of acceptor to donor densities of states. We introduce $E_{\rm GB}$ as the neutral energy level of the distribution of states: the grain boundary charge is zero when the gap states are filled to this level[15]. If the Fermi level is above (below) $E_{\rm GB}$, the grain boundary core develops a negative (positive) charge. At thermal equilibrium, the continuum of gap states can therefore be mapped onto an effective *single* defect level positioned at energy $E_{\rm GB}$. The defect charge is then

$$Q_{\rm GB} = qN_{\rm GB}(1-2f_0) \quad (6)$$

where f_0 is now the effective occupancy of the effective single donor+acceptor defect state $E_{\rm GB}$. This latter case was studied in details in Ref. 13. This mapping is valid for values of α such that the densities of donor and acceptor states remain commensurate[16]. In the large defect density limit (specified below) we find that $E_{\rm GB} = E_g/(1+\alpha)$.

We consider large defect densities of states such that $Q_{\rm GB}/(qN_{\rm GB}) \ll 1$. We show in Appendix A that the critical defect density of states for this condition to be satisfied is

$$N^{\rm crit}_{\rm GB} = \frac{1+e^3}{q}\sqrt{8\epsilon q N_A(E_{\rm GB}-E_F+3k_BT)}. \quad (7)$$

for the single donor state, and

$$\rho^{\rm crit}_D = \frac{1}{q}\left(\frac{e+1}{e-1}\right)\frac{\sqrt{8\epsilon q N_A(E_{\rm GB}-E_F)}}{E_g}, \quad (8)$$

for the continuum of acceptor and donor states. For material parameters typical of CdTe, Eq. (7) is on the order of 10^{12} cm^{-2} for $E_{\rm GB} \in [0.4\ {\rm eV}, 1.3\ {\rm eV}]$, and Eq. (8) ranges from 3×10^{11} cm$^{-2}\cdot$eV^{-1} to 10^{12} cm$^{-2}\cdot$eV^{-1} for $\alpha \in [0.1, 4]$.

III. EQUILIBRIUM PROPERTIES AND ASSUMPTIONS AWAY FROM EQUILIBRIUM

A. Equilibrium properties

We first provide an expression for the equilibrium built-in potential $V^0_{\rm GB}$ in terms of the defect occupancy f_0. In both single donor and continuum defect cases, the absence of recombination at thermal equilibrium gives the equilibrium carrier densities along the grain boundary[17]

$$n^{\rm eq}_{\rm GB} = \frac{f_0}{1-f_0}\bar{n}_{\rm GB}(E_{\rm GB}) \quad (9)$$

$$p^{\rm eq}_{\rm GB} = \frac{1-f_0}{f_0}\bar{p}_{\rm GB}(E_{\rm GB}) \quad (10)$$

We take the energy reference at the valence band edge in the grain interior of the p-type material, as shown in Fig. 1(c). With this reference, the distance between the Fermi level and the conduction band at the grain boundary core is $E_g - E_F - qV^0_{\rm GB}$. This determines another form of the equilibrium electron density at the grain boundary core, $n^{\rm eq}_{\rm GB} = N_C\exp[(E_F - E_g + qV^0_{\rm GB})/k_BT]$. Equating this form with Eq. (9) leads to the equilibrium grain boundary built-in potential

$$qV^0_{\rm GB} = E_{\rm GB} - E_F + k_BT\ln\left(\frac{f_0}{1-f_0}\right). \quad (11)$$

We next consider the determination of the defect state occupancy in equilibrium f_0. The value of f_0 is determined by electroneutrality: the grain boundary charge must be compensated by the charge of the surrounding depletion region. The depletion region width surrounding the grain boundary in the p-type region is $W_{\rm GB} = \sqrt{2\epsilon V^0_{\rm GB}/(qN_A)}$ as shown in Fig. 1 (the schematic neglects the modification of the grain boundary built-in potential in the pn junction depletion region). For the donor case, the electroneutrality requirement leads to the following equation for f_0:

$$\frac{1}{8}\left(\frac{N_{\rm GB}}{N_A L_D}\right)^2(1-f_0)^2 = \frac{E_{\rm GB}-E_F}{k_BT} + \ln\left(\frac{f_0}{1-f_0}\right), \quad (12)$$

where $L_D = \sqrt{\epsilon k_BT/qN_A}$. In general Eq. (12) must be solved numerically for f_0. Since no closed form of f_0 is

available, we present our results in terms of the variable f_0. Note that as $N_{\rm GB} \to \infty$, $f_0 \to 1$ and the built-in potential of Eq. (11) diverges logarithmically. In practice, realistic values of $N_{\rm GB}$ are well below this diverging limit, so this issue can be safely ignored. In the continuum defect case, $f_0 = 1/2$ for the assumed large value of $N_{\rm GB}$. In this case, Eq. (11) reduces to the previously studies single donor+acceptor case of Ref. 13.

B. Assumptions in the nonequilibrium analysis

A direct analytical solution for the full two-dimensional problem is not feasible. To make analytical progress, we focus on the solutions along the grain boundary core, reducing the problem to one dimension. The reduction of the problem from 2D to 1D is possible because electrons are electrostatically confined to the grain boundary core. In turn, the current along the grain boundary is carried by electrons.[8,13,18] Our approach relies on approximations (or assumptions) which render the continuity/Poisson equations analytically tractable. In this section we state our assumptions and sketch out the subsequent solution procedures.

One blanket assumption is that the hole quasi-Fermi level is approximately flat across and along the grain boundary. This is valid because the hole current along the grain boundary is negligible (electrons carry the current along the grain boundary), while in the grain interior holes are majority carriers. We provide a criterion restricting the validity of this assumption in Appendix B. We find that for typical material parameters of CdTe, this assumption is generally valid for large bulk hole mobilities.

The next assumption is that the grain boundary charge does not change with voltage. This is justified by the limit of high defect density of states $Q_{\rm GB}(V)/(qN_{\rm GB}) \ll 1$. This assumption is crucial as it enables us to relate the electrostatic potential to the quasi-Fermi levels without the Poisson equation. We denote f the nonequilibirum counterpart of f_0 in Eqs. (5) and (6). f is an integral of Eq. (2) and depends on the nonequiblirium carrier densities. Fixing the grain boundary charge to its equilibrium value results in assuming $f = f_0$. The relative sizes of the terms in Eq. (2) delineate three regimes of different behavior:

"n-type" grain boundary: In this case, the defect occupancy is determined by the electron carrier density at the grain boundary. f remains fixed by maintaining a constant distance between electron quasi-Fermi level and (actual or effective) $E_{\rm GB}$. We further assume that the electron quasi-Fermi level is relatively flat and equal to its bulk value. This is valid because the high electron density in the grain boundary core enables high currents with relatively small quasi-Fermi level gradients. Together with the assumption of the relatively flat hole quasi-Fermi level, the densities and recombination are easily determined.

"p-type" grain boundary: In this case, the occupancy of the defect state(s) is determined by the hole carrier density at the grain boundary. f remains fixed by maintaining a constant distance between the hole quasi-Fermi level and (actual or effective) $E_{\rm GB}$. Because the electron density is small at the grain boundary core, the electron quasi-Fermi level develops gradients to drive the electron current along the grain boundary. In this case we must solve a one-dimensional diffusion equation for the electron density to obtain the carrier densities and recombination.

High recombination: For sufficiently large applied voltages, the electron and hole carrier densities are the largest terms in the expression for f and determine the defect occupancy. In the donor case, maintaining $f = f_0$ leads to the following relation between electron and hole density:

$$S_p p_{\rm GB} \approx (1 - f_0) S_n n_{\rm GB}. \tag{13}$$

In the continuum case, the occupancy of the acceptor and donor states are constrained to ensure that $f \approx 1/2$. Because f is now an integral of the acceptor and donor occupancies, a simple relation like Eq. (13) does not exist. We show in Sec. V C that $f = 1/2$ leads to the relation:

$$p_{\rm GB} = \gamma(V) n_{\rm GB} \tag{14}$$

where the density ratio γ varies weakly with voltage. In this high-recombination regime, Eq. (13) or Eq. (14) together with the assumption of flat hole quasi-Fermi level leads to a one-dimensional drift-diffusion equation for electrons confined to the grain boundary. Solving this equation leads to the carrier densities and recombination.

A final assumption which applies for all of our analysis is that the grains are not fully depleted, i.e. grain sizes d are greater than $2W_{\rm GB}$. For a doping density 10^{15} cm^{-3} this requirement implies $d > 2$ μm. The average grain size in CdTe thin films (excluding twin boundaries) was recently[19] found to be 2.3 μm.

IV. GRAIN BOUNDARY DARK CURRENT OF A SINGLE DONOR DEFECT STATE

We begin with the case of a single donor state in the gap of the absorber material. The grain boundary charge is proportional to $1 - f_0$ (see Eq. (5)). In the limit of large defect density of states, the electroneutrality of the grain boundary is satisfied when the defect level is fully occupied: $f_0 \approx 1$. In the n-region ($x < x_0$) the large concentration of electrons satisfies this requirement without

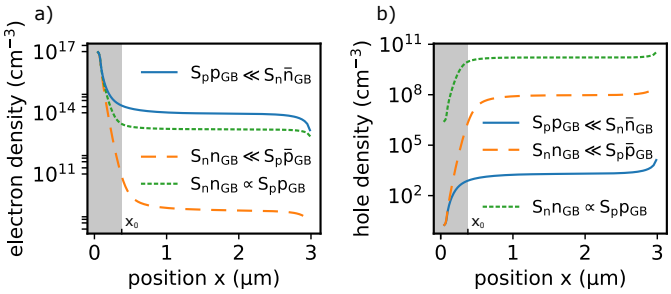

FIG. 2. Numerical simulation results for carrier densities along the grain boundary for the three regimes determined by the ratio $S_n n_{GB}$ to $S_p \bar{p}_{GB}$. (a) Electron density. (b) Hole density. $S_n n_{GB} \gg S_p \bar{p}_{GB}$ was obtained for $E_{GB} = 1$ eV at $V = 0.3$ V (blue continuous lines), $S_n n_{GB} \ll S_p \bar{p}_{GB}$ for $E_{GB} = 0.5$ eV at $V = 0.3$ V (orange dashed lines) and $S_n n_{GB} \propto S_p p_{GB}$ for $E_{GB} = 0.5$ eV at $V = 0.7$ V (green dotted lines). All calculations were done for $S_n = S_p = 10^5$ cm/s, $\mu_n = \mu_p = 200$ cm^2/(V · s) and $N_A = 10^{15}$ cm^{-3}. General parameters are listed in Table II.

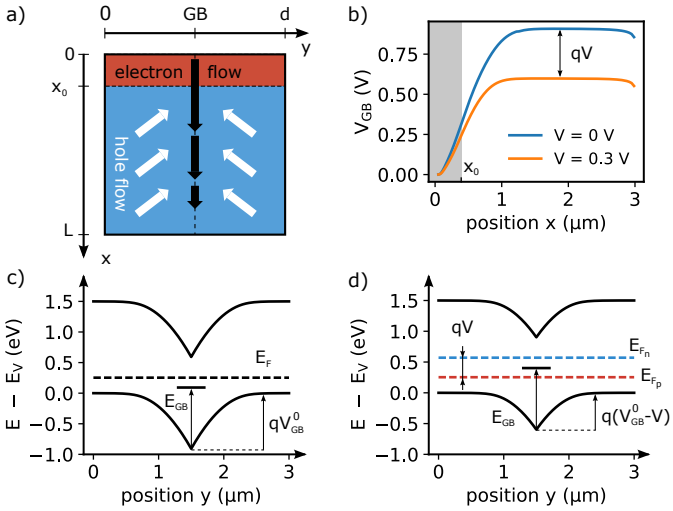

FIG. 3. (a) Schematic of the electron and hole currents in the regime $S_p p_{GB} \ll S_n \bar{n}_{GB}$. (b) Difference in electrostatic potential between grain boundary and grain interior V_{GB} along the grain boundary for the applied voltages $V = 0$ V and $V = 0.3$ V. (c) and (d) Band diagrams across the grain boundary for $x > x_0$, for $V = 0$ V and $V = 0.3$ V respectively.

the need for modifying the electrostatics around the grain boundary. In the p-region, however, the resulting built-in potential around the grain boundary is given by Eq. (11)

$$qV^0_{GB} = E_{GB} - E_F - k_B T \ln(1 - f_0). \tag{15}$$

Because of the logarithm term and $f_0 \approx 1$, the Fermi level E_F is not pinned to E_{GB}.

We now derive analytical expressions for the dark recombination current at the grain boundary. We support the physical descriptions with numerically computed carrier densities along the grain boundary presented in Fig. 2. The absence of modification of the electrostatics in the n-region results in a recombination similar to the grain interior of the pn junction depletion region: the recombination is determined by the hole density (minority carrier density) which decreases sharply for $x < x_0$, as shown in Fig. 2(b). In what follows we therefore neglect the contribution of this part of the grain boundary to the total recombination, and focus on carrier densities and recombination for $x \geq x_0$. The general expression for the grain boundary recombination current reads

$$J_{GB}(V) = \frac{1}{d} \int_{x_0}^{L_{GB}} \int_0^d \mathrm{d}x\mathrm{d}y \; R_{GB}(x, y), \tag{16}$$

where L_{GB} is the length of the grain boundary. R_{GB} is the recombination at the grain boundary and has the Schockley-Read-Hall form

$$R_{GB}(x, y) = \frac{S_n S_p (n_{GB}(x) p_{GB}(x) - n_i^2) \delta(y - y_{GB})}{S_n (n_{GB}(x) + \bar{n}_{GB}) + S_p (p_{GB}(x) + \bar{p}_{GB})}, \tag{17}$$

where n_i is the intrinsic carrier density and we dropped the "donor" superscript for the recombination velocities. $\bar{n}_{GB}$ and $\bar{p}_{GB}$ are given by Eqs. (3) and (4) evaluated at $E = E_{GB}$.

As discussed in Sec. III, under nonequilibrium conditions we assume that the grain boundary carrier densities evolve while keeping the level occupancy equal to its thermal equilibrium value f_0. This assumption together with the energy of the defect state leads to three regimes of interest for the grain boundary dark current. We next analyze these regimes individually.

A. Grain boundary recombination for $S_p p_{GB} \ll S_n \bar{n}_{GB}$

We first consider $S_p p_{GB} \ll S_n \bar{n}_{GB}$, also called "$n$-type" regime. As discussed in Sec. III, for this case f_0 remains fixed by keeping $E_{F_n} - E_{GB}$ constant. Equivalently, E_{F_n} replaces E_F in Eq. (15)[13]. In the grain interior of the p-region, the increase of voltage V shifts the electron quasi-Fermi level from the valence band by an amount qV. Assuming that E_{F_n} is flat across the grain boundary[20], the built-in potential also varies with V:

$$\begin{aligned} qV_{GB} &= E_{GB} - E_{F_n} - k_B T \ln(1 - f_0) \\ &= E_{GB} - E_F - qV - k_B T \ln(1 - f_0) \\ &= q(V^0_{GB} - V), \end{aligned} \tag{18}$$

where E_F is the equilibrium Fermi level. Equation (18) shows that the grain boundary built-in potential decreases linearly with voltage for $x > x_0$. This is shown in Fig. 3(b). The reduction of the barrier allows holes of the grain interior to flow toward the grain boundary core. The recombination of holes generates an electron current along the grain boundary, as depicted in Fig. 3(a).

Using Eq. (18) and the assumption of flat hole quasi-Fermi level[21], the distance between E_{F_p} and the valence band is $E_{\rm GB} - qV - k_BT\ln(1-f_0)$. The hole density at the grain boundary therefore reads

$$p_{\rm GB}(x > x_0) = (1-f_0)N_V e^{(-E_{\rm GB}+qV)/k_BT}. \quad (19)$$

The hole density is shown in Fig. 2(b) (blue continuous lines). The electron density is equal to its equilibrium value Eq. (9) for $x > x_0$, shown in Fig. 2(a). Because $S_n n_{\rm GB}$ is much larger than all the other terms in the denominator of Eq. (17), the recombination simplifies to

$$R_{\rm GB}(x > x_0) = S_p p_{\rm GB}(x > x_0) \quad (20)$$

for $V \gg k_BT/q$. The recombination is uniform for $x > x_0$ and negligible in the n-region, so the dark recombination current reads

$$J_{\rm GB}(V) = (1-f_0)\frac{S_p(L_{\rm GB}-x_0)}{d}N_V e^{(-E_{\rm GB}+qV)/k_BT}. \quad (21)$$

The features of Eq. (21) are a saturation current $(1-f_0)S_p(L_{\rm GB}-x_0)/d$, an ideality factor of 1, and an activation energy $E_{\rm GB}$.

In Appendix B we derive a condition under which the hole quasi-Fermi level is approximately flat. This condition reads ($V_T = k_BT/q$)

$$\frac{S_p}{2\mu_p}\sqrt{\frac{2\epsilon}{qV_TN_A}} < 1. \quad (22)$$

For $S_{n,p} = 10^5$ cm/s, $N_A = 10^{15}$ cm^{-3}, $\epsilon = 9.4\ \epsilon_0$, $V_T = 25$ meV, Eq. (22) is satisfied for $\mu_p > 32$ cm^2/(V·s). Over the course of this work, we found this numerical value to be an acceptable threshold for all the grain boundary regimes of this section.

B. Grain boundary recombination for $S_n n_{\rm GB} \ll S_p \bar{p}_{\rm GB}$

We turn to $S_n n_{\rm GB} \ll S_p \bar{p}_{\rm GB}$, also called "$p$-type" regime. In this case the distance between $E_{\rm GB}$ and E_{F_p} does not change with the applied voltage V, as seen in Figs. 4(c) and (d). We further assume that E_{F_p} is flat equal to E_F[21]. As a result Eq. (15) shows that the grain boundary built-in potential is independent of the applied voltage for $x > x_0$. This is shown in Fig. 4(b).

The electron transport is more complex than in the previous case. In particular, the electron quasi-Fermi level is not always equal to $E_F + qV$ along the grain boundary, but varies significantly to accommodate an electron current. The grain boundary built-in potential confines electrons near the grain boundary core, leading to a one-dimensional motion along it. As a result, the continuity equation around the grain boundary reduces

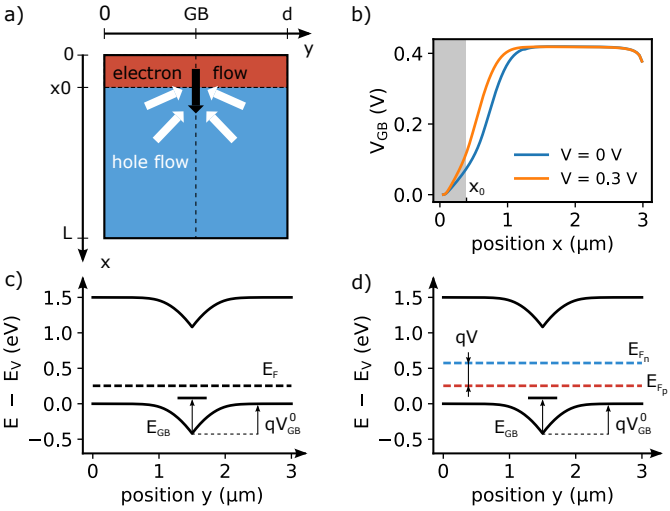

FIG. 4. (a) Schematic of the electron and hole currents in the regime $S_n n_{\rm GB} \ll S_p \bar{p}_{\rm GB}$. (b) Difference in electrostatic potential between grain boundary and grain interior $V_{\rm GB}$ along the grain boundary for the applied voltages $V = 0$ V and $V = 0.3$ V. (c) and (d) Band diagrams across the grain boundary for $x > x_0$, for $V = 0$ V and $V = 0.3$ V respectively.

to a one-dimensional equation along the grain boundary core (x-direction). Upon solving this equation beyond x_0 (see Appendix C), the electron density reads

$$n_{\rm GB}(x > x_0) = \frac{N_C}{1-f_0}e^{(-E_g+E_{\rm GB}+qV)/k_BT}e^{-\frac{x-x_0}{L_n}}, \quad (23)$$

where $L_n = \sqrt{2D_nL_{\mathcal{E}}/(S_n(1-f_0))}$ ($D_n = k_BT\mu_n/q$: electron diffusion coefficient) is the diffusion length of electrons along the grain boundary. $L_{\mathcal{E}}$ is the length scale of the confinement of the electrons to the grain boundary core. This length is related to $\mathcal{E}_y$, the electric field transverse to the grain boundary in the neutral region of the pn junction, by $2L_{\mathcal{E}} = 2k_BT/\mathcal{E}_y$ (see Eq. (69) in Appendix C). The electron density described here is shown in Fig. 2(a) (dashed orange line). The hole density (shown in Fig. 2(b)) is equal to its equilibrium value Eq. (10). Because $S_p\bar{p}_{\rm GB}$ dominates the denominator of Eq. (17), the recombination reads

$$R_{\rm GB}(x > x_0) = (1-f_0)S_n n_{\rm GB}(x > x_0) \quad (24)$$

for $V \gg k_BT/q$. We now consider two limiting cases for the integration of the recombination.

The first limit is the large diffusion length, $L_n \gg L_{\rm GB}$, obtained for large mobilities and small values of recombination velocity. The electron density is uniform for $x > x_0$, leading to the dark recombination current

$$J_{\rm GB}(V) = \frac{S_n(L_{\rm GB}-x_0)}{d}N_C e^{(-E_g+E_{\rm GB}+qV)/k_BT}. \quad (25)$$

In the second limit, $L_n \ll L_{\rm GB}$, the electron mobility is small so that the electron density decays rapidly beyond

x_0. The recombination is peaked on both sides of x_0 and the recombination current reads

$$J_{\rm GB}(V) = \frac{S_n L_n}{d} N_C e^{(-E_g + E_{\rm GB} + qV)/k_B T}. \quad (26)$$

The description of this regime is shown in Fig. 4(a). Holes converge to x_0 where they recombine, generating a localized electron current. Both regimes have similar features: the saturation current varies as $S_n N_C/d$, the ideality factor is 1 and the thermal activation energy is $E_g - E_{\rm GB}$.

C. Grain boundary recombination for $S_n n_{\rm GB} \approx (1-f_0) S_p p_{\rm GB}$

As we increase the applied voltage in either of the previous cases, $S_n \bar{n}_{\rm GB}$ and $S_p \bar{p}_{\rm GB}$ become negligible compared to $S_p p_{\rm GB}$ and $S_n n_{\rm GB}$ respectively. Because the system approximately maintains the level occupancy close to its thermal equilibrium value, the carrier densities satisfy the relation

$$f_0 \approx \frac{S_n n_{\rm GB}}{S_n n_{\rm GB} + S_p p_{\rm GB}}. \quad (27)$$

Equation (27) leads to $S_p p_{\rm GB} \approx (1-f_0) S_n n_{\rm GB}$, defining the "high-recombination" regime.

While the electrostatic potential now varies along the grain boundary, the built-in potential still confines the electron to a one-dimensional motion along the grain boundary core. Similarly to the regime $S_n n_{\rm GB} \ll S_p \bar{p}_{\rm GB}$, a one-dimensional continuity equation controls the electron transport along the grain boundary. Upon solving this equation (see Appendix D), we find the carrier densities

$$n_{\rm GB}(x > x_0) = \frac{1}{\sqrt{1-f_0}} \sqrt{\frac{S_p}{S_n}} n_i e^{qV/(2k_B T)} e^{-\frac{x-x_0}{L'_n}} \quad (28)$$

$$p_{\rm GB}(x > x_0) = \sqrt{1-f_0} \sqrt{\frac{S_n}{S_p}} n_i e^{qV/(2k_B T)} e^{-\frac{x-x_0}{L'_n}}, \quad (29)$$

where $L'_n = \sqrt{4 D_n L'_{\mathcal{E}}/(S_n(1-f_0))}$ ($L'_{\mathcal{E}}$ is the characteristic length of the electric field across the grain boundary). These densities yield the grain boundary recombination

$$R_{\rm GB}(x > x_0) = \sqrt{1-f_0} \sqrt{S_n S_p} n_i e^{qV/(2k_B T)} e^{-\frac{x-x_0}{L'_n}} \quad (30)$$

for $V \gg k_B T/q$. We consider two limiting cases for the recombination current.

Because of the factor $1-f_0$ in L'_n, common material parameters for CdTe lead to large diffusion lengths such that $L'_n \gg L_{\rm GB}$. The uniform grain boundary (for $x > x_0$) described in Sec. IV A applies in this case, and the recombination current reads

$$J_{\rm GB}(V) = \sqrt{1-f_0} \frac{\sqrt{S_n S_p}(L_{\rm GB} - x_0)}{d} n_i e^{qV/(2k_B T)}. \quad (31)$$

Param.	Value	Param.	Value
L	3 μm	ϵ	9.4 ϵ_0
d	3 μm	$\tau_{n,p}$	(10 to 100) ns
N_C	8×10^{17} cm^{-3}	$S_{n,p}$	(1 to 10^6) cm/s
N_V	1.8×10^{19} cm^{-3}	$N_{\rm GB}$	10^{14} cm^{-2}
E_g	1.5 eV	$\mu_{n,p}$	(10 to 5×10^3) cm^2/(V $\cdot$ s)
N_D	10^{17} cm^{-3}	N_A	(10^{14} to 10^{16}) cm^{-3}

TABLE II. List of default parameters (param.) for numerical simulations.

For smaller values of the electron diffusion length, $L'_n \ll L_{\rm GB}$ and the recombination is peaked at x_0 with the electron and hole flows depicted in Fig. 4(a). The dark recombination current therefore reads

$$J_{\rm GB}(V) = \sqrt{1-f_0} \frac{\sqrt{S_n S_p} L'_n}{d} n_i e^{qV/(2k_B T)}. \quad (32)$$

In both limits the thermal activation energy is $E_g/2$ and the ideality factor is 1. Note that the factor $1-f_0$ is on the order of 10^{-4} to 10^{-3} for typical doping densities. As a result, S_n is effectively reduced by two orders of magnitude, therefore significantly reducing the amplitude of the grain boundary recombination current. This difference between the single donor case and the single acceptor+donor state studied in Ref. 13 comes from the difference in defect capture rates of electrons and holes in each case. The occupancy of the defect energy level is skewed towards large electron occupancy for the single donor state, while it is balanced between electrons and holes for the mixture donor/acceptor. As a result an electron *and* a hole are more likely to be captured together by the defect in the mixture donor/acceptor. The recombination current is therefore higher in the donor/acceptor case.

D. Numerical verification of the analytical results

We verify the accuracy of our analytical results using numerical solutions of the drift-diffusion-Poisson equations for our geometry in Fig. 1(a). Table II gives the list of material parameters used for these calculations.

Fig. 5 presents calculations for the grain boundary dark current. At each applied voltage the current is given by the smallest value between the n-type, p-type and high recombination regimes.

The doping density is varied in Fig. 5(a) for $E_{\rm GB} = 0.5$ eV. The crossover from the p-type regime ($S_n n_{\rm GB} \ll S_p \bar{p}_{\rm GB}$) to the high recombination regime ($S_n n_{\rm GB} \approx (1-f_0) S_p p_{\rm GB}$) occurs at about 0.5 V, as seen from the slope change. The inset shows the doping dependence of the high recombination regime. Contrary to the case studied in Ref. 13 where common material parameters for CdTe lead to decreasing grain boundary dark currents with doping at high voltages, the donor state shows

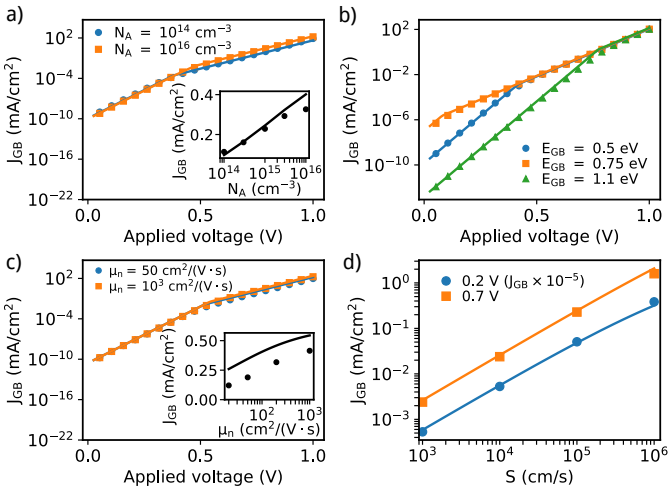

FIG. 5. Grain boundary recombination current characteristics $J_{\rm GB}(V)$ for a single donor state at $E_{\rm GB} = 0.5$ eV (p-type grain boundary), $S_n = S_p = 10^5$ cm/s and $\mu_n = 200$ cm^2/(V $\cdot$ s) unless specified otherwise. Symbols are numerical calculations, full lines correspond to analytical results Eqs. (21), (75) and (84). (a) $\mu_n = 200$ cm^2/(V $\cdot$ s). Inset: grain boundary recombination current as a function of doping density at $V = 0.7$ V. (b) $\mu_n = 200$ cm^2/(V $\cdot$ s), $N_A = 10^{15}$ cm^{-3}. (c) $N_A = 10^{16}$ cm^{-3}. Inset: grain boundary recombination current as a function of electron mobility for $V = 0.7$ V (high recombination regime). (d) Grain boundary recombination current as a function of surface recombination velocity ($S_n = S_p$), at $V = 0.2$ V (dots) and $V = 0.7$ V (squares).

the opposite behavior. The key difference between these cases lies in the effective electron surface recombination velocity entering the definition of the electron diffusion length at high voltages. In the single acceptor+donor case it is given by $S_n/2$, while in the single donor case we found $(1 - f_0)S_n$. Because $f_0 \approx 1$ the latter value is orders of magnitude smaller than the former. The primary consequence is that for the same S_n, the diffusion length is much larger in the donor case. In turn, the limit $L_n' \gg L_{\rm GB}$ is the relevant one for common CdTe parameters with the single donor state (Eq. (31)), while the opposite limit is relevant for the case studied in Ref. 13. An increasing doping density increases the depletion charge, leading to a larger value of $1 - f_0$. Consequently the $1 - f_0$ factor in Eq. (31) is responsible for the increase in recombination current with doping density observed here. This is a major difference that will reflect in the open-circuit voltage.

We show the various regimes in Fig. 5(b), where $E_{\rm GB} = 0.5$ eV and $E_{\rm GB} = 1.1$ eV correspond respectively to a p-type and n-type grain boundary at equilibrium. Figure 5(c) shows the dependence of the grain boundary dark current with mobility. This dependence is absent at low voltage, as shown by the limiting case Eq. (25). At higher voltages, the relevant limit is Eq. (31), as discussed above, which is independent of mobility. This explains the weak mobility dependence shown in the inset.

Finally, Fig. 5(d) shows the scalings of the grain boundary dark current with surface recombination velocity. We show grain boundary dark currents in the p-type regime (dots) and high-recombination regime (squares). On this plot both scalings are equal. The dark current scales as S_p at low voltage, and as $\sqrt{S_n S_p}$ at high voltage. The second scaling is given by Eq. (31) which is the relevant limit in this case. With $S_n = S_p$ these scalings are identical.

V. GRAIN BOUNDARY DARK RECOMBINATION CURRENT OF A CONTINUUM OF DEFECT STATES

We turn to the case of a continuum of donor and acceptor states in the absorber band gap. We assume densities of states uniform in energy: $\rho_D = N_{\rm GB}/E_g$, $\rho_A(E) = \alpha N_{\rm GB}/E_g$, where

$$\alpha = \rho_A/\rho_D \tag{33}$$

determines the ratio of acceptor to donor densities of states. More acceptor (donor) states leads to p-type (n-type) grain boundary core. The neutral energy level of the distribution of gap states is $E_{\rm GB} = E_g/(1 + \alpha)$ (see Sec. II).

Under nonequilibrium conditions the grain boundary dark current is given by Eq. (16) where the integral along the grain boundary (x-direction) now starts from $x = 0$. The recombination is the sum of the contributions from the acceptor and donor states (represented by the superscript $k \in (A, D)$)

$$R^k_{\rm GB}(x) = \int_0^{E_g} \frac{{\rm d}E}{E_g} \frac{S^k_n S^k_p (n_{\rm GB} p_{\rm GB} - n_i^2)}{S^k_n (n_{\rm GB} + \bar{n}_{\rm GB}(E)) + S^k_p (p_{\rm GB} + \bar{p}_{\rm GB}(E))}. \tag{34}$$

Despite the apparent complexity of a continuum of states as opposed to a single state, the physical description of the nonequilibrium electron and hole currents is the same as given in Ref. 13. This apparent complexity will be incorporated in effective surface recombination velocities in what follows. The results of Ref. 13 and of this section are gathered in the last two rows of Table I.

A. Grain boundary recombination for $S^k_n n_{\rm GB} \gg S^k_p p_{\rm GB}$

We begin with the regime $S^k_n n_{\rm GB} \gg S^k_p p_{\rm GB}$ (n-type grain boundary). In this regime the electron quasi-Fermi level is pinned to $E_g/(1+\alpha)$. The recombination is determined by holes, which flow from the p-type grain interior into the grain boundary core. Because most of the absorber is p-type, the recombination is uniform along the

entire grain boundary. We refer to Sec. III A of Ref. 13 for a more complete description of this regime.

The electron density is independent of voltage and spatially uniform, given by Eq. (9) with $f_0 = 1/2$. The hole density is also uniform and reads

$$p_{\mathrm{GB}} = N_V e^{(-E_{\mathrm{GB}}+qV)/k_BT}. \tag{35}$$

The grain boundary dark current reads

$$J_{\mathrm{GB}}(V) = \frac{\mathcal{S}_p L_{\mathrm{GB}}}{d} N_V e^{(-E_{\mathrm{GB}}+qV)/k_BT} \tag{36}$$

where $\mathcal{S}_p$ is the effective surface recombination velocity

$$\mathcal{S}_p = \sum_{k\in A,D} S_p^k \int_0^{E_g} \frac{\mathrm{d}E}{E_g} \frac{1}{1+\frac{\bar{n}_{\mathrm{GB}}(E)}{n_{\mathrm{GB}}}+\frac{S_p^k \bar{p}_{\mathrm{GB}}(E)}{S_n^k \bar{n}_{\mathrm{GB}}}}. \tag{37}$$

The integrals in Eq. (37) can be computed analytically but the results are cumbersome and difficult to interpret. To give a sense of these integrals, we refer to Fig. 6(b) where we show the grain boundary recombination as a function of energy. This figure shows that only states with energies $E_g - E_{\mathrm{GB}} \lesssim E \lesssim E_{\mathrm{GB}}$ contribute significantly to the recombination. The upper limit results from the fact that states above E_{GB} are empty of electrons. The lower limit is the energy at which holes are emitted from the defect state to the valence band faster than electrons relax from the conduction band to the defect state. This rapid hole emission rate prevents recombination. The typical width of the integrand of $\mathcal{S}_p$ is

$$\Delta_k(\alpha) = \left| \frac{1-\alpha}{1+\alpha} + \frac{k_BT}{E_g} \ln\left(\frac{S_n^k}{S_p^k}\frac{N_C}{N_V}\right)\right| \tag{38}$$

as shown on the continuous plot of Fig. 6(b). Equation (37) therefore simplifies to

$$\mathcal{S}_p \approx S_p^A \Delta_A(\alpha) + S_p^D \Delta_D(\alpha). \tag{39}$$

Note that the occupancy of the gap states is independent of the applied voltage in this regime (see the continuous curve in Fig. 6(a)). That is because the occupancy of the gap states is determined solely by the electron density, which is independent of voltage here.

In Appendix B we derive a condition under which the hole quasi-Fermi level is approximately flat. This condition applied here reads ($V_T = k_BT/q$)

$$\frac{\mathcal{S}_p}{2\mu_p}\sqrt{\frac{2\epsilon}{qV_T N_A}} < 1. \tag{40}$$

For $\alpha = 2$, $S_{n,p}^{A,D} = 10^5$ cm/s, $N_A = 10^{16}$ cm^{-3}, $\epsilon = 9.4\ \epsilon_0$, $V_T = 25$ meV, Eq. (40) is satisfied for $\mu_p > 450$ cm^2/(V $\cdot$ s). This value is in the upper range of standard bulk mobilities for CdTe because of the increase of recombination amplitude compared to a single defect state problem. We found this order of magnitude to be an acceptable threshold for all the grain boundary regimes with the continuum of defect states.

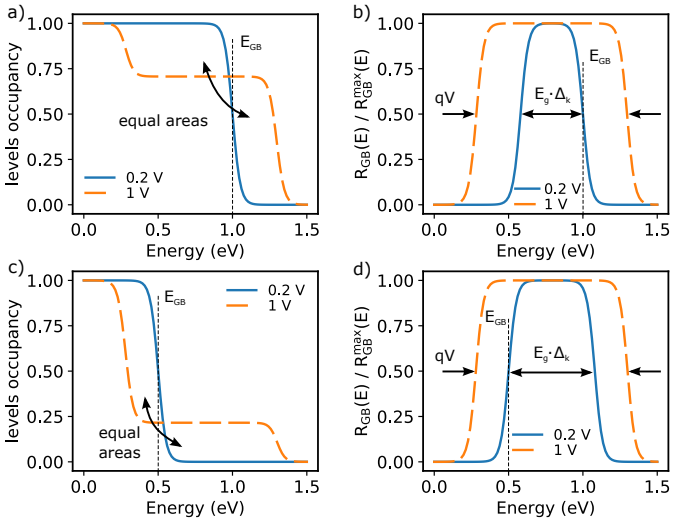

FIG. 6. (a), (c) Occupancy of the gap states as a function of energy at x_0 for $\rho_A/\rho_D = 0.5$ ($E_{\mathrm{GB}} = 1$ eV) and $\rho_A/\rho_D = 2$ ($E_{\mathrm{GB}} = 0.5$ eV) respectively. (b), (d) Normalized recombination at x_0 as a function of energy corresponding to the occupancy levels in (a) and (c) respectively. We used $S_{n,p}^A = S_{n,p}^D$ so that recombinations of the acceptor and donor states are the same.

B. Grain boundary recombination for $S_n^k n_{\mathrm{GB}} \ll S_p^k p_{\mathrm{GB}}$

In the regime $S_n^k n_{\mathrm{GB}} \ll S_p^k p_{\mathrm{GB}}$ (p-type grain boundary), the hole quasi-Fermi level is pinned to $E_g/(1+\alpha)$. In this regime the recombination is determined by electrons flowing into the grain boundary core from regions of the grain interior where $n > p$. This corresponds to $x < x_0$ in Fig. 1(a). The recombination is therefore mainly concentrated within the n- region of the pn junction depletion region, and is uniform for $x < x_0$. We refer to Sec. III B of Ref. 13 for a complete description of this case.

For $x > x_0$, the hole density is uniform given by Eq. (10) with $f_0 = 1/2$; the electrons are confined to the grain boundary core by the grain boundary built-in electric field, leading to a one-dimensional diffusion along it. Solving the one-dimensional diffusion equation leads to the electron density

$$\begin{aligned} n_{\mathrm{GB}}(x) &= N_C e^{(-E_g+E_{\mathrm{GB}})/k_BT} e^{qV/k_BT} && \text{for } x < x_0 \\ &= N_C e^{(-E_g+E_{\mathrm{GB}})/k_BT} e^{qV/k_BT} e^{-\frac{x-x_0}{L_n}} && \text{for } x > x_0 \end{aligned} \tag{41}$$

where $L_n = \sqrt{2D_nL_{\mathcal{E}}/\mathcal{S}_n}$ (D_n: electron diffusion coefficient) is the electron diffusion length, and $L_{\mathcal{E}} = k_BT/\mathcal{E}_y$ is the length scale of the confinement ($\mathcal{E}_y$: electric field transverse to the grain boundary in the bulk of the pn junction). $\mathcal{S}_n$ is the effective surface recombination ve-

locity in this case

$$\mathcal{S}_n = \sum_{k\in A,D} S_n^k \int_0^{E_g} \frac{\mathrm{d}E}{E_g} \frac{1}{1+\frac{\bar{p}_{\mathrm{GB}}(E)}{p_{\mathrm{GB}}}+\frac{S_n^k \bar{n}_{\mathrm{GB}}(E)}{S_p^k \bar{p}_{\mathrm{GB}}}}. \quad (42)$$

The grain boundary dark current reads

$$J_{\mathrm{GB}}(V) = \frac{\mathcal{S}_n}{d} N_C e^{(-E_g+E_{\mathrm{GB}}+qV)/k_BT} \times \left[x_0 + L_n\left(1-e^{-\frac{L_{\mathrm{GB}}-x_0}{L_n}}\right)\right], \quad (43)$$

The integrals in $\mathcal{S}_p$ have a similar interpretation as for the n-type grain boundary: only the states with energies $E_{\mathrm{GB}} \lesssim E \lesssim E_g - E_{\mathrm{GB}}$ contribute significantly to the recombination, as shown in Fig. 6(d). The lower limit results from the fact that states below E_{GB} are empty of holes. The upper limit is the energy at which electrons are emitted from the defect state to the conduction band faster than holes relax from the valence band to the defect state. The integrands in $\mathcal{S}_n$ exhibit the same shape as $\mathcal{S}_p$. In particular, the width of the integrand is still given by Eq. (38). Equation (42) therefore simplifies to

$$\mathcal{S}_p \approx S_n^A \Delta_A(\alpha) + S_n^D \Delta_D(\alpha). \quad (44)$$

Similarly to the n-type grain boundary, the occupancy of the gap states is determined solely by holes and is therefore independent of the applied voltage, shown in Fig. 6(c).

C. Grain boundary recombination for $n_{\mathrm{GB}} \propto p_{\mathrm{GB}}$

As the applied voltage is increased above $E_g\Delta_k/q$, the minority carrier density approaches the majority carrier density at the grain boundary. This results in a rearrangement of the gap states occupancies. However, we use the assumption that the grain boundary charge does not change with voltage, as discussed in Sec. III, which leads to the constraint

$$1 = 1/E_g \int_0^{E_g} \mathrm{d}E\ f_D(E) + \alpha f_A(E). \quad (45)$$

The change in occupancies keeps the area under the occupancy curves equal to its equilibrium value, as shown by the dashed lines in Figs. 6(a) and (c). More specifically, occupancies above E_{GB} increase while the ones below E_{GB} decrease. These changes lead to an increase of the number of states contributing to the recombination as can be seen in Figs. 6(b) and (d).

There is no pinning of either quasi-Fermi level to $E_g/(1+\alpha)$ in this regime. We refer to Sec. III C of Ref. 13 for the derivations in this case. We can show that the constraint Eq. (45) imposes that the ratio of carrier densities remains constant along the grain boundary. While this ratio was independent of voltage for the single acceptor+donor state of Ref. 13, this not the case anymore. Assuming $p_{\mathrm{GB}} = \gamma(V) n_{\mathrm{GB}}$, and solving a one-dimensional diffusion equation along the grain boundary leads to the carrier densities

$$n_{\mathrm{GB}}(x) = \frac{1}{\sqrt{\gamma}} n_i e^{qV/(2k_BT)} e^{-\frac{x}{L_n'}} \quad (46)$$

$$p_{\mathrm{GB}}(x) = \sqrt{\gamma} n_i e^{qV/(2k_BT)} e^{-\frac{x}{L_n'}}. \quad (47)$$

We find $\gamma(V)$ by solving the self-consistent equation Eq. (45). This ratio gives the value of the plateau reached by the levels occupancy at energies around midgap, as shown by the dashed lines in Figs. 6(a) and (c). Because n_{GB} and p_{GB} dominate the level occupancy Eq. (2) at these energies, the value of the plateau is $1/(1+\gamma\beta_k)$, with $\beta_k = S_p^k/S_n^k$. Considering (unrealistically) large values of applied voltage such that the levels occupancy is entirely independent of energy, we find that γ converges to

$$\gamma = \frac{\alpha - 1 + \sqrt{(1-\alpha)^2 + 4\alpha\beta_A/\beta_D}}{2\beta_A}. \quad (48)$$

In Eqs. (46) and (47), $L_n' = \sqrt{4D_n L_{\mathcal{E}}'/\mathcal{S}}$ is the diffusion length of electrons along the grain boundary, and $L_{\mathcal{E}}'$ is the characteristic length of the electric field transverse to the grain boundary. The effective surface recombination velocity $\mathcal{S}$ reads

$$\mathcal{S} = \sum_{k\in A,D} \frac{\gamma S_n^k S_p^k}{S_n^k + \gamma S_p^k} \int_0^{E_g} \frac{\mathrm{d}E}{E_g} \frac{1}{1+\frac{S_n^k \bar{n}_{\mathrm{GB}}(E) + S_p^k \bar{p}_{\mathrm{GB}}(E)}{(S_n^k+\gamma S_p^k)\frac{n_i}{\sqrt{\gamma}} e^{qV/(2k_BT)}}}. \quad (49)$$

The integrand of Eq. (49) now varies with voltage as shown by the dashed line in Fig. 6(b). It can be shown that an approximation for the integral is

$$\mathcal{S} \approx \sum_{k\in A,D} \frac{\gamma S_n^k S_p^k}{S_n^k + \gamma S_p^k} \left[\frac{qV}{E_g} - \frac{2k_BT}{E_g} \ln\left(\frac{\sqrt{\gamma} S_n^k}{S_n^k + \gamma S_p^k}\right)\right]. \quad (50)$$

Gathering the above results leads to the grain boundary dark current

$$J_{\mathrm{GB}}(V) = \frac{\mathcal{S} L_n'}{\sqrt{\gamma} d} n_i e^{V/(2V_T)} \left[1 - e^{-L_{\mathrm{GB}}/L_n'}\right]. \quad (51)$$

This result is formally similar to the corresponding case for the single acceptor+donor state studied in Ref. 13, yet the voltage dependence of the effective surface recombination velocity is a key difference. Taking $S_{n,p}^A = S_{n,p}^D$, Eq. (51) is proportional to $\sqrt{\alpha}/(1+\alpha)$. This shows that when the distribution of gap states is skewed towards either donors or acceptors (e.g. big or small α), the recombination current is diminished. This reduction can be understood with the levels occupancy in Fig. 6(c) (dashed line). The recombination plotted in Fig. 6(d) shows that the states around midgap contribute the most to the recombination. These states correspond to the plateau of the levels occupancy, which is approximately equal to $1/(1+\alpha)$ here. For large or small α, the plateau is far

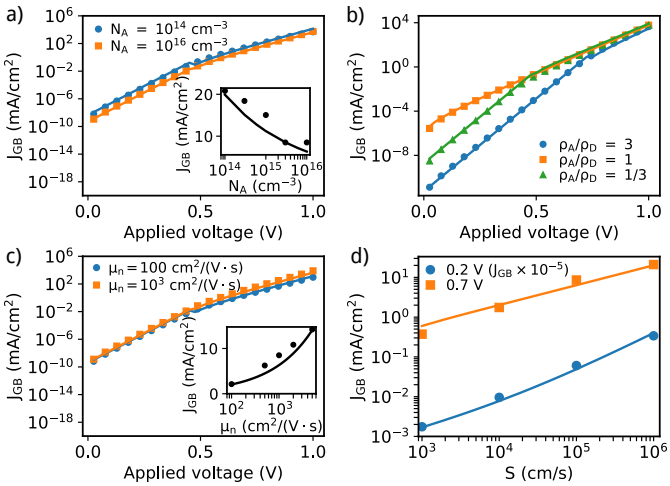

FIG. 7. Grain boundary recombination current characteristics $J_{\rm GB}(V)$ for a continuum of donor and acceptor states with $\rho_A/\rho_D = 2$, $S^A_{n,p} = S^D_{n,p} = 10^5$ cm/s and $\mu_n = 10^3$ cm^2/(V · s) unless specified otherwise. Symbols are numerical calculations, full lines correspond to analytical results. (a) $\mu_n = 10^3$ cm^2/(V · s). Inset: grain boundary recombination current as a function of doping density at $V = 0.7$ V. (b) $\mu_n = 10^3$ cm^2/(V · s), $N_A = 10^{16}$ cm^{-3}. (c) $N_A = 10^{16}$ cm^{-3}. Inset: grain boundary recombination current as a function of electron mobility for $V = 0.7$ V. (d) Grain boundary recombination current as a function of surface recombination velocity ($S^A_{n,p} = S^D_{n,p}$), at $V = 0.2$ V (dots) and $V = 0.7$ V (squares).

from 1/2, which reduces the probability that a hole *and* an electron be captured together by a gap state. This reduced probability leads to a reduction of the recombination current.

D. Numerical verification of the analytical results

The numerical tests to verify the accuracy of the results of this section are presented in Fig. 7. These results were obtained with $S^A_{n,p} = S^D_{n,p}$. For applied voltages below $E_g\Delta_k/q$, the current is given by the smallest value between the n-type and p-type regimes. For higher values of applied voltage we used the high recombination regime. For all plots except Fig. 7(b) we used $\rho_A/\rho_D = 2$, which leads to $E_{\rm GB} = 0.25$ eV (p-type grain boundary).

We vary the doping density in Fig. 7(a). Before the change of slope, the dark current is given by Eq. (43) which exhibits a doping dependence mostly via the width of the n-region x_0. The reduction of the slope reveals the crossover to the high recombination regime ($n_{\rm GB} \propto p_{\rm GB}$) where the dark current is given by Eq. (51). In this regime, the inset shows the predicted scaling in $N_A^{-1/4}$.

Fig. 7(b) shows the grain boundary dark current for various ratios ρ_A/ρ_D. In descending order, these correspond to grain boundary neutral levels $E_{\rm GB} \approx 0.38$ eV, 0.75 eV and 1.1 eV. The crossover to the high recombination regime occurs when the occupancy of the gap states starts to change significantly, that is for $qV > E_g\Delta_k$ (see Fig. 6(b) and (d)).

The dependence of the dark current with mobility is shown in Fig. 7(c). At low voltage, this dependence is barely visible but present. The dependence is weak in the p-type regime because both limiting cases of Eq. (43), $L_n \ll L_{\rm GB}$ and $L_n \gg L_{\rm GB}$, are independent of mobility. The chosen set of parameters lies in between these limits. At high voltages we verify the square root scaling as shown by Eq. (51) in the limit $L'_n \ll L_{\rm GB}$. Increasing mobility reduces the suppression of carrier densities away from the maximum of recombination by increasing the electron diffusion length. This in turn increases the recombination along the grain boundary.

Fig. 7(d) shows the scalings of the grain boundary dark current with surface recombination velocity $S^{A,D}_{n,p}$. Because we used equal surface recombination velocities for the donor and acceptor states, and electrons and holes, the effective recombination velocities and $S^{A,D}_{n,p}$ are proportional . The notable feature of this plot is the $\sqrt{\mathcal{S}}$ scaling of the grain boundary recombination current obtained at high voltage. This feature only appears at high recombination velocities as it requires $L'_n \ll L_{\rm GB}$, as shown by Eq. (51). In the opposite limit one recovers a linear scaling in $\mathcal{S}$.

VI. OPEN-CIRCUIT VOLTAGE

We now consider a charged grain boundary under illumination and derive relations for the open-circuit voltage $V_{\rm oc}$. We assume that around $V_{\rm oc}$ the current voltage relation under illumination is given by the sum of the short circuit current $J_{\rm sc}$ and the dark current (see Sec. V of Ref. 13 for a discussion on the validity of this assumption). The dark current is the sum of the grain boundary dark current (derived in Sec. III and Sec. IV) and the bulk recombination current. We use the results of Sec. IV of Ref. 13 for the bulk recombination whenever necessary.

Neglecting the bulk recombination and the non-exponential voltage dependences in the grain boundary dark currents, we can write down explicit forms for the open-circuit voltage associated with the grain boundary recombination. The general form of the open-circuit voltage reads

$$qV_{\rm oc}^{\rm GB} = nE_a + nk_BT \ln\left(\frac{dJ_{\rm sc}}{S\lambda N}\right), \qquad (52)$$

where S is a surface recombination velocity, λ is a length characteristic of the physical regime, N is an effective density of states, E_a is an activation energy, V is the applied voltage and n is an ideality factor. Even though Eq. (52) is not mathematically correct in all cases (because it neglects non-exponential voltage dependence), it captures the dominant scalings for the physical parameters and should give the reader an intuition for how

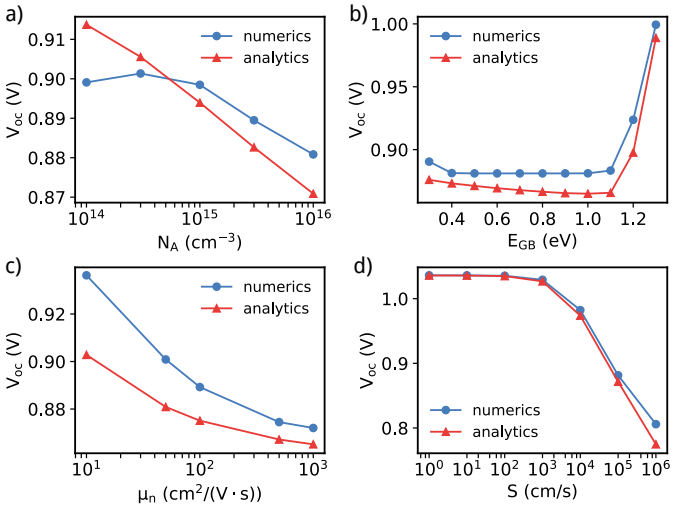

FIG. 8. Open-circuit voltage for the system described in Fig. 1(a) with a single donor state at $E_{\rm GB} = 0.5$ eV, with $\tau_n = 100$ ns, under a photon flux 10^{21} m$^{-2} \cdot$ s^{-1}. The absorption length is 2.3×10^4 cm^{-1}. The carriers mobility is 200 cm^2/(V $\cdot$ s), $N_A = 10^{16}$ cm^{-3} and $S_n = S_p = 10^5$ cm/s unless specified otherwise. Numerical data are in blue (dots) and analytical predictions are in red (triangles). (a) $V_{\rm oc}$ as a function of doping density. (b) $V_{\rm oc}$ as a function of the defect state energy level. (c) $V_{\rm oc}$ as a function of electron and hole mobility (assumed equal). (d) $V_{\rm oc}$ as a function of surface recombination velocity ($S_n = S_p$).

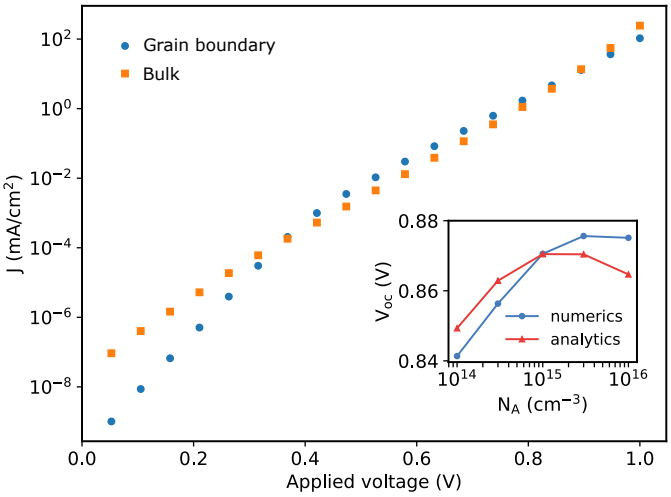

FIG. 9. Recombination current as a function of voltage for the grain boundary (blue dots) and the bulk (orange squares) obtained with a bulk lifetime $\tau_n = 10$ ns. Other parameters: $N_A = 10^{15}$ cm^{-3}, $S_{n,p} = 10^5$ cm/s, $\mu_{n,p} = 200$ cm^2/(V $\cdot$ s), $E_{\rm GB} = 0.5$ eV. Inset: open-circuit voltage for our system under a photon flux 10^{21} m$^{-2} \cdot$ s^{-1}. The absorption length is 2.3×10^4 cm^{-1}.

these parameters impact $V_{\rm oc}$. The parameters entering Eq. (52) are shown in Table I for all grain boundary configurations.

A. Single donor state

We begin with the single donor state in the gap of the absorber material. The parameters in Eq. (52) for this case are given in the first row of Table I. Fig. 8 shows comparisons between the numerically computed $V_{\rm oc}$, and the values obtained with the numerically computed $J_{\rm sc}$ and the analytic forms of the dark current.

These results differ somewhat from the single state study of Ref. 13. As we discussed in Sec. IV D, the single donor state with common material parameters for CdTe exhibits increasing grain boundary dark currents with doping at high voltages. As a result, $V_{\rm oc}$ decreases with doping as shown in Fig. 8(a). Figure 8(b) shows that the open-circuit voltage as a function of defect energy level is not symmetrical from midgap. In fact, for $E_{\rm GB} \gtrsim 1.2$ eV the open-circuit voltage is given by the grain boundary recombination current of the n-type regime Eq. (21), while for lower $E_{\rm GB}$ values, the open-circuit voltage is given by the regime $S_n n_{\rm GB} \approx (1-f_0) S_p p_{\rm GB}$ and Eq. (31) (high recombination regime). Figure 5(b) shows that, for a given applied voltage, the amplitude of the grain boundary recombination current of the n-type regime is smaller than the one of the high recombination regime (hence the larger $V_{\rm oc}$ in the first case). Figure 8(c) shows the dependence with mobility for values higher than 100 cm^2/(V $\cdot$ s). Under the chosen conditions the grain boundary recombination current depends weakly on mobility. Finally the logarithmic dependence on surface recombination velocity of Eq. (52) is shown in Fig. 8(d).

A key difference between this single donor case and the donor+acceptor case of Ref. 13 is the amplitude of the grain boundary recombination in the high recombination regime. In the single donor state of the present work, the electron surface recombination velocity is effectively reduced by the factor $1 - f_0$ (which can be on the order of 10^{-3} in the regime of large defect density of states) as can be seen in the expressions of the carrier densities Eqs. (28) and (29), as well as in the recombination itself Eq. (30). As a result, for intermediate values of bulk lifetime (≈ 10 ns), the bulk recombination current is of the same order of magnitude as the grain boundary recombination current with $S_{n,p} = 10^5$ cm/s, as shown in Fig. 9. In this example, reducing the doping density increases the bulk recombination (because the width of the pn junction depletion region increases) which now dominates over the grain boundary contribution. The inset of Fig. 9 shows that the resulting open-circuit voltage increases with doping, contrary to the behavior shown in Fig. 8(a) for which $\tau = 100$ ns.

B. Continuum of gap states

We now turn to the continuum of acceptor and donor states. The parameters in Eq. (52) are given in the last row of Table I. Note that in the high recombination regime ($n_{\rm GB} = \gamma p_{\rm GB}$), Eq. (52) applies when neglecting the linear voltage dependence of the effective surface recombination velocity $\mathcal{S}$ (see Eq. (50)). Despite this approximation, Eq. (52) provides the correct overall scalings with doping density, distribution of states, mobility and surface recombination velocities. Fig. 10 shows the comparisons of the simulated open-circuit voltages with our analytical results.

The continuum of states studied here has lots of features similar to the single acceptor+donor state studied in Ref. 13. In particular we find the same scalings of $V_{\rm oc}$ with doping and mobility, shown in Fig. 10(a) and (c). The amplitudes of the open-circuit voltage presented here are smaller than for the single state problem, due to the increased number of states which contribute to the recombination. This explains why the logarithmic dependence of the $V_{\rm oc}$ with the surface recombination velocity occurs for smaller values than for a single state, as shown in Fig. 10(d).

A difference with Ref. 13 is the U-shape dependence of $V_{\rm oc}$ with the ratio ρ_A/ρ_D, presented in Fig. 10(b). The open-circuit voltage now varies with ρ_A/ρ_D (i.e. with the effective single state value) even for intermediate values of the ratio. This is because the grain boundary recombination current in the high recombination regime depends on this ratio via γ as shown by Eq. (48).

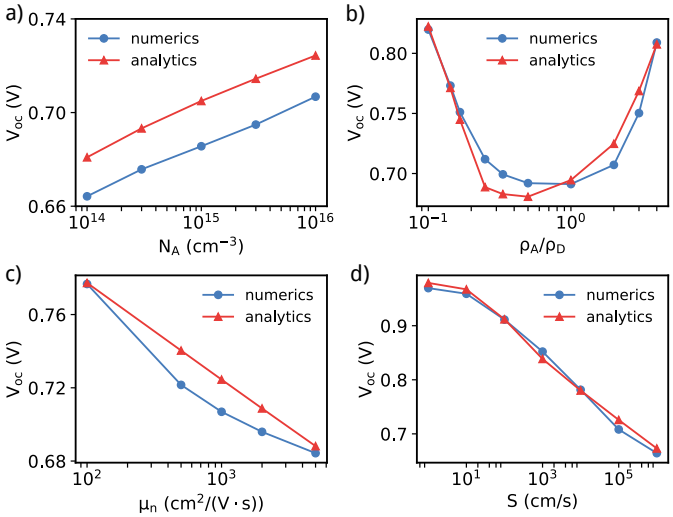

FIG. 10. Open-circuit voltage for the system described in Fig. 1(a) with a continuum of donor and acceptor states with $\rho_A/\rho_D = 2$, under a photon flux 10^{21} m$^{-2}\cdot$s^{-1}. The absorption length is 2.3×10^4 cm^{-1}. The carriers mobility is 10^3 cm^2/(V$\cdot$s), $N_A = 10^{16}$ cm^{-3} and $S_n = S_p = 10^5$ cm/s unless specified otherwise. Numerical data are in blue (dots) and analytical predictions are in red (triangles). (a) $V_{\rm oc}$ as a function of doping density. (b) $V_{\rm oc}$ as a function of the ratio of acceptor and donor densities of states. (c) $V_{\rm oc}$ as a function of electron and hole mobility (assumed equal). (d) $V_{\rm oc}$ as a function of surface recombination velocity ($S_n = S_p$).

VII. CONCLUSION

We generalized the physical descriptions associated with the microscopic charge transport and recombination of Ref. 13 to two additional configurations of gap states: a single donor state and a continuum of donor and acceptor states. In this work we derived the corresponding analytic expressions for the grain boundary dark recombination current. We found that all these configurations share three similar regimes describing the grain boundary dark recombination current as a function of voltage (n-type, p-type and high-recombination). However, they exhibit differences in the amplitude of the subsequent recombinations. Mixtures of acceptor and donor states (single level and continuum) result in enhanced recombination that reduces the open-circuit voltage for a wide range of bulk lifetimes. The amplitudes of recombination for the single donor state are lower, and commensurate with the bulk recombination for intermediate bulk lifetimes.

ACKNOWLEDGMENTS

B. G. acknowledges support under the Cooperative Research Agreement between the University of Maryland and the National Institute of Standards and Technology Center for Nanoscale Science and Technology, Award 70NANB14H209, through the University of Maryland.

Appendix A CONDITIONS FOR LARGE DEFECT DENSITY REGIME

We derive the minimal defect densities for which $Q_{\rm GB}/(qN_{\rm GB}) \ll 1$ for the single donor defect state and the continuum of defect states. Because the defect statistics in thermal equilibrium are different in each case (see Eq. (5) and Eq. (6) respectively), we must derive two different criteria.

We start with the single donor state. The condition $Q_{\rm GB}/(qN_{\rm GB}) \ll 1$ requires that $f_{\rm GB} \approx 1$. We specify this requirement by imposing that the Fermi level lies at least $3k_BT$ above the defect level at the grain boundary,

$$E_F + qV^0_{\rm GB} - E_{\rm GB} > 3k_BT. \tag{53}$$

This condition together with Eq. (11) imposes

$$1 - f_0 > \frac{1}{1+e^3}, \tag{54}$$

where $f_0 = (1 + \exp[(E_{\rm GB} - E_F)/k_BT])^{-1}$. Using a depletion approximation and $qV^0_{\rm GB} = E_{\rm GB} - E_F + 3k_BT$, the charge in the depleted regions surrounding the grain boundary is

$$Q = \sqrt{8\epsilon q N_A V^0_{\rm GB}} \approx \sqrt{8\epsilon q N_A (E_{\rm GB} - E_F + 3k_BT)}. \tag{55}$$

Equating Eq. (5) and Eq. (55) leads to the critical defect density of states

$$N^{\rm crit}_{\rm GB} = \frac{1+e^3}{q}\sqrt{8\epsilon q N_A (E_{\rm GB} - E_F + 3k_BT)}. \tag{56}$$

For the case of the continuum of acceptor and donor states, we use the mapping onto a single state problem where the charge at the grain boundary is given by Eq. (6). Here we simply use the criterion derived in Appendix A of Ref. 13 and find the critical donor density

$$\rho^{\rm crit}_D = \frac{1}{q}\left(\frac{e+1}{e-1}\right)\frac{\sqrt{8qN_A(E_{\rm GB} - E_F)}}{E_g}, \tag{57}$$

where $E_{\rm GB} = E_g/(1+\alpha)$ with $\alpha = \rho_D/\rho_A$. This critical donor density of states depends on the ratio α considered. Also note that because of the division by E_g, $\rho^{\rm crit}_D$ is a density of states per energy unit (expressed in $\mathrm{m}^{-2}\cdot\mathrm{eV}^{-1}$).

Appendix B CONDITION FOR NEARLY FLAT HOLE QUASI-FERMI LEVEL

We specify the domain of validity of the assumption of flat hole quasi-Fermi level. In the main text we consider $E_{F_p} = E_F$ when variations of E_{F_p} across the grain boundary are smaller than k_BT. An expansion of E_{F_p} across the grain boundary yields

$$E_{F_p} = E_F - \left|\frac{\partial E_{F_p}}{\partial y}\right|\delta y, \tag{58}$$

where the gradient of E_{F_p} at the grain boundary depends on the regime considered (e.g. n-type grain boundary). The single donor state and the continuum of defect states require formally the same condition. The relevant surface recombination velocity must be used in each case. We are able to derive such a criterion only for an n-type grain boundary but found that it applies well also in other regimes. In what follows we focus on the single donor state.

In the regime $S_p p_{\rm GB} \ll S_n \bar{n}_{\rm GB}$, the gradient of E_{F_p} is obtained by integrating the continuity equation for holes across the grain boundary over an infinitely small distance,

$$\left|\frac{\partial E_{F_p}}{\partial y}\right| = q\frac{S_p}{2\mu_p}p_{\rm GB}. \tag{59}$$

Assuming that the variation of E_{F_p} across the grain boundary follows that of the electrostatic potential, the distance across the grain boundary where $E_F - E_{F_p} < k_BT$ is given by a depletion approximation $\delta y = \sqrt{2\epsilon V_T/(qN_A)}$. The assumption of flat E_{F_p} is therefore valid for

$$\frac{S_p}{2\mu_p}\sqrt{\frac{2\epsilon}{qV_TN_A}} < 1. \tag{60}$$

For the continuum of states one would use $\mathcal{S}_p$ instead.

Appendix C DERIVATIONS FOR p-TYPE DONOR DEFECT STATE

Using the energy scale and definitions of Fig. 4(d), the carrier densities at the grain boundary are given by

$$n_{\rm GB}(x) = N_C e^{(E_{F_n}(x) + q\phi_{\rm GB}(x) - E_g)/k_BT}, \tag{61}$$

$$p_{\rm GB}(x) = N_V e^{(-E_{F_p}(x) - q\phi_{\rm GB}(x))/k_BT}, \tag{62}$$

where $\phi_{\rm GB}$ is the electrostatic potential at the grain boundary. The zero of electrostatic potential is at the p-contact away from the grain boundary. In the p-type donor state, the electrostatic potential is uniform along the grain boundary in the bulk of the pn junction and is independent of voltage. The value of $\phi_{\rm GB}$ is determined by the grain boundary built-in potential at thermal equilibrium,

$$q\phi_{\rm GB} = qV^0_{\rm GB}, \tag{63}$$

where $V^0_{\rm GB}$ is given by Eq. (15). The grain boundary recombination is maximum at x_0, where x_0 is the point where the carrier densities in the grain interior are equal. We consider that the grain interior recombination is peaked at the same point. Using a depletion approximation in the depletion region of the pn junction in the grain interior, we find that $n = p = n_i$ at

$$x_0 = \sqrt{\frac{2\epsilon V_{\rm bi}}{qN_A}}\left[1 - \sqrt{1 - \frac{V_T}{V_{\rm bi}}\ln\left(\frac{N_D}{n_i}\right)}\right], \tag{64}$$

where $V_{\rm bi}$ is the pn junction built-in potential (the dependence of x_0 on applied voltage is weak and can be neglected). Using the potential Eq. (63) in Eqs. (61) and (62), and assuming that $E_{F_p} = E_F$[21], we obtain expressions for the carrier densities beyond x_0,

$$n_{\rm GB}(x \geq x_0) = \frac{N_C}{1-f_0}e^{(-E_g + E_{\rm GB})/k_BT}e^{(E_{F_n}(x) - E_F)/k_BT}, \tag{65}$$

$$p_{\rm GB}(x \geq x_0) = (1-f_0)N_V e^{-E_{\rm GB}/k_BT}. \tag{66}$$

Despite the above formulation, these relations are valid only for $x \gg x_0$. We extend their domain of validity to $x = x_0$ for the purpose of calculating the recombination, where the errors we make here on $n_{\rm GB}$ and $p_{\rm GB}$ cancel out.

For $x \geq x_0$ we use the continuity equation for electrons to obtain E_{F_n},

$$\frac{\partial J_{n,x}}{\partial x} + \frac{\partial J_{n,y}}{\partial y} = S_n(1-f_0)n_{\rm GB}\delta(y-y_{\rm GB}) + R_{\rm bulk}(y), \tag{67}$$

where $R_{\rm bulk}$ is the bulk recombination and the electron current component along the grain boundary is given by

$$J_{n,x}(x,y) = \mu_n n_{\rm GB}(x) e^{-y/L_\mathcal{E}} \frac{\partial E_{F_n}}{\partial x}(x). \tag{68}$$

In the above equation we assumed that the electron density across the grain boundary decays as $e^{-y/L_\mathcal{E}}$, where

$$L_\mathcal{E} = V_T\sqrt{2\epsilon/(qN_A V^0_{\rm GB})} \tag{69}$$

is the characteristic length associated with the electric field transverse to the grain boundary in the bulk region. This exponential decay assumes that E_{F_n} is flat around the grain boundary, which coincides with the fact that the currents going to the grain boundary are small. Integrating Eq. (67) in the y-direction around the grain boundary leads to

$$2L_\mathcal{E}\mu_n k_B T \frac{\partial^2}{\partial x^2}\left[e^{E_{F_n}/k_BT}\right] = qS_n(1-f_0)e^{E_{F_n}/k_BT}, \tag{70}$$

where we neglected the currents in the y-direction at the end of the grain boundary depletion region, and the bulk recombination. We introduce the effective diffusion length $L_n = \sqrt{2D_nL_\mathcal{E}/(S_n(1-f_0))}$, where $D_n = k_BT\mu_n/q$ is the electron diffusion constant, to rewrite Eq. (70) as

$$\frac{\partial^2}{\partial x^2}\left[e^{E_{F_n}/k_BT}\right] = \frac{1}{L_n^2}e^{E_{F_n}/k_BT}. \tag{71}$$

Considering that $E_{F_n} = E_F + qV$ at $x = x_0$, and neglecting the diverging part of the solution of Eq. (71), we obtain

$$E_{F_n}(x \geq x_0) = E_F + qV - k_BT\frac{x-x_0}{L_n}. \tag{72}$$

We verify the accuracy of Eq. (72) in Fig. 11(b) (blue dotted curve).

Inserting Eq. (72) into Eq. (65) yields the electron density given in the main text

$$n_{\rm GB}(x \geq x_0) = \frac{N_C}{1-f_0}e^{(-E_g+E_{\rm GB}+qV)/k_BT}e^{-\frac{x-x_0}{L_n}}. \tag{73}$$

Because $S_n n_{\rm GB} \ll S_p\bar{p}_{\rm GB}$, the recombination at the grain boundary reads

$$R_{\rm GB}(x \geq x_0) = S_n(1-f_0)n_{\rm GB}(x \geq x_0). \tag{74}$$

We integrate over the length of the grain boundary to obtain the recombination current

$$J_{\rm GB}(V) = \frac{S_nN_C}{d}e^{(-E_g+E_{\rm GB}+qV)/k_BT}L_n\left[1-e^{-\frac{L_{\rm GB}-x_0}{L_n}}\right]. \tag{75}$$

Equation (75) is the general result in the case $S_n n_{\rm GB} \ll S_p\bar{p}_{\rm GB}$.

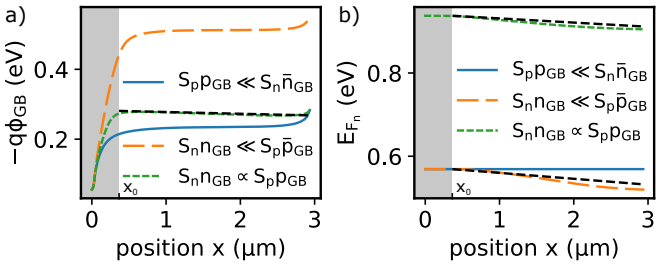

FIG. 11. Numerical data computed along the grain boundary for the densities presented in Fig. 2 with the mobility $\mu_{n,p} = 20\ \mathrm{cm}^2/(\mathrm{V}\cdot\mathrm{s})$. (a) Electrostatic potential. The dark dashed line corresponds to Eq. (82). (b) Electron quasi-Fermi level. The dark dashed lines correspond to Eq. (80) (upper) and Eq. (72) (lower).

Appendix D DERIVATIONS FOR DONOR STATE IN THE HIGH RECOMBINATION REGIME

Here we provide the derivations of the analytical results presented in Sec. IV C. In the high recombination regime there is a constant k such that $S_pp_{\rm GB} = kS_nn_{\rm GB}$ along the grain boundary. In addition $n_{\rm GB}p_{\rm GB} = n_i^2e^{(E_{F_n}-E_{F_p})/k_BT}$, so that we get

$$n_{\rm GB}(x) = \sqrt{\frac{S_p}{kS_n}}n_i e^{(E_{F_n}(x)-E_{F_p}(x))/(2k_BT)}. \tag{76}$$

Similarly to the p-type case, the recombination is peaked at x_0 and decays after that point so we focus the derivation beyond x_0.

From here on the derivation of E_{F_n} follows the exact same steps as Appendix C starting with the continuity equation:

$$\frac{\partial J_{n,x}}{\partial x} + \frac{\partial J_{n,y}}{\partial y} = \frac{k}{1+k}S_nn_{\rm GB}\delta(y-y_{\rm GB}) + R_{\rm bulk}(y) \tag{77}$$

where $L'_\mathcal{E} = \sqrt{2\epsilon V_T/(qN_A)}$. $L'_\mathcal{E}$ is the characteristic length associated with the electric field transverse to the grain boundary. $R_{\rm bulk}$ is again the bulk recombination. Because the grain boundary built-in potential is not uniform in this regime, the transverse electric field depends on the location along the grain boundary. While $L'_\mathcal{E}$ does not correspond to a precise field, we find that it accurately determines the slopes of the electron quasi-Fermi level and the electrostatic potential along the grain boundary. The electron current is still given by Eq. (68) with the change of $L_\mathcal{E}$ for $L'_\mathcal{E}$. Integrating Eq. (77) around the grain boundary leads to

$$4L'_\mathcal{E}\mu_n k_BT\frac{\partial^2}{\partial x^2}\left[e^{\frac{E_{F_n}-E_{F_p}}{2k_BT}}\right] = q\frac{k}{1+k}S_ne^{\frac{E_{F_n}-E_{F_p}}{2k_BT}}, \tag{78}$$

where we neglected the currents in the y-direction at the end of the grain boundary depletion region, and the bulk recombination. We introduce the effective diffusion

length $L'_n = \sqrt{4D_n L'_{\mathcal{E}}(1+k)/(kS_n)}$, and assume that $E_{F_p} = E_F$[21] to rewrite Eq. (78) as

$$\frac{\partial^2}{\partial x^2}\left[e^{E_{F_n}/(2k_BT)}\right] = \frac{1}{{L'_n}^2} e^{E_{F_n}/(2k_BT)}. \tag{79}$$

Considering that $E_{F_n} = E_F + qV$ at $x = x_0$ we obtain

$$E_{F_n}(x \geq x_0) = E_F + qV - 2k_BT\frac{x - x_0}{L'_n}. \tag{80}$$

Since $kS_n n_{\rm GB} = S_p p_{\rm GB}$, we can equate Eqs. (61) and (62) to get

$$E_{F_n}(x) = -2q\phi_{\rm GB}(x) - E_F - E_g - k_BT\ln\left(k\frac{S_nN_C}{S_pN_V}\right), \tag{81}$$

which yields the electrostatic potential along the grain boundary

$$\phi_{\rm GB}(x) = k_BT\frac{x - x_0}{L'_n} - E_F - q\frac{V}{2} - k_BT\ln\left(\frac{n_i}{N_V}\sqrt{\frac{kS_n}{S_p}}\right). \tag{82}$$

Comparisons of Eq. (80) and Eq. (82) with numerical data are shown in Figs. 11(a) and 11(b) respectively (green solid curves). We see that the numerically computed potential and electron quasi-Fermi level are not linear over the entire length of the grain boundary, however the analytical results give a good approximation of the slopes near the depletion region.

Inserting Eqs. (80) and (82) into the densities Eqs. (61) and (62) yields the densities given in Sec. IV C. These densities yield the grain boundary recombination

$$R_{\rm GB}(x > x_0) = \frac{\sqrt{kS_nS_p}}{1+k} n_i e^{qV/(2k_BT)} e^{-\frac{x-x_0}{L'_n}}. \tag{83}$$

Integrating the recombination over the length of the grain boundary gives the recombination current

$$J_{\rm GB}(V) = \frac{\sqrt{kS_nS_p}L'_n}{(1+k)d} n_i e^{V/(2V_T)}\left[1 - e^{-L_{\rm GB}/L'_n}\right]. \tag{84}$$

Equation (84) is the general result in the case $kS_n n_{\rm GB} = S_p p_{\rm GB}$.

The constant k can be specified considering that the occupancy of the grain boundary defect level remains equal to its thermal equilibrium value f_0. We thus find

$$k \approx 1 - f_0, \tag{85}$$

assuming that $f_0 \lesssim 1$ because of the high defect density of states.

[1] S. G. Kumar and K. K. Rao, Energy Environ. Sci. **7**, 45 (2014).
[2] A. Polman, M. Knight, E. C. Garnett, B. Ehrler, and W. C. Sinke, Science **352** (2016).
[3] M. A. Green, K. Emery, Y. Hishikawa, W. Warta, E. D. Dunlop, D. H. Levi, and A. W. Y. Ho-Baillie, Prog. Photovolt. Res. Appl. **25**, 3 (2017).
[4] R. M. Geisthardt, M. Topič, and J. R. Sites, IEEE J. Photovolt. **5**, 1217 (2015).
[5] H. P. Yoon, P. M. Haney, D. Ruzmetov, H. Xu, M. S. Leite, B. H. Hamadani, A. A. Talin, and N. B. Zhitenev, Sol. Energ. Mat. Sol. Cells **117**, 499 (2013).
[6] H. Moutinho, R. Dhere, C.-S. Jiang, Y. Yan, D. Albin, and M. Al-Jassim, J. Appl. Phys. **108**, 074503 (2010).
[7] M. Tuteja, P. Koirala, V. Palekis, S. MacLaren, C. S. Ferekides, R. W. Collins, and A. A. Rockett, J. Phys. Chem. C **120**, 7020 (2016).
[8] M. Gloeckler, J. R. Sites, and W. K. Metzger, J. Appl. Phys. **98**, 113704 (2005).
[9] K. Taretto and U. Rau, J. Appl. Phys. **103**, 094523 (2008).
[10] U. Rau, K. Taretto, and S. Siebentritt, Appl. Phys. A **96**, 221 (2009).
[11] F. Troni, R. Menozzi, E. Colegrove, and C. Buurma, J. Electron. Mater. **42**, 3175 (2013).
[12] R. M. Geisthardt, M. Topič, and J. R. Sites, IEEE J. Photovolt. **5**, 1217 (2015).
[13] B. Gaury and P. M. Haney, J. Appl. Phys. **120**, 234503 (2016).
[14] W. Shockley and W. T. Read, Phys. Rev. **87**, 835 (1952).
[15] E. H. Rohderick, *Metal-semiconductor contacts* (Oxford Univ. Press, 1978).
[16] We will restrict α to the interval $[0.1, 4]$.
[17] The general net recombination rate for electrons at the grain boundary core is $r = S_n(1-f_0)n_{\rm GB} - S_n f_0 \bar{n}_{\rm GB}(E_{\rm GB})$. At thermal equilibrium this rate is zero which gives Eq. (9). The same reasoning applies for holes and leads to Eq. (10).
[18] M. Tuteja, A. B. Mei, V. Palekis, A. Hall, S. MacLaren, C. S. Ferekides, and A. A. Rockett, J. Phys. Chem. Lett. **7**, 4962 (2016).
[19] J. Moseley, W. K. Metzger, H. R. Moutinho, N. Paudel, H. L. Guthrey, Y. Yan, R. K. Ahrenkiel, and M. M. Al-Jassim, J. Appl. Phys. **118**, 025702 (2015).
[20] The electron current transverse to the grain boundary is small compared to the longitudinal one. So despite the low electron density in the grain interior, the gradient of E_{F_n} across the grain boundary driving the transverse current is small and can be neglected.
[21] Because holes are majority carriers in the bulk of the absorber, the hole quasi-Fermi level is flat equal to E_F there. We derived in Appendix B a criterion under which the hole quasi-Fermi level is flat across the grain boundary, so that the bulk quasi-Fermi level extends to the grain boundary core.